J Mater Sci (2008) 43:6546–6555
DOI 10.1007/s10853-008-2802-z

Influence of processing on the microstructure of Cu–8Cr–4Nb

L. G. Vettraino · J. L. Heelan · C. A. Faconti · J. L. Walley · A. Garg · J. R. Groza · J. C. Gibeling

Received: 29 November 2007 / Accepted: 11 June 2008 / Published online: 10 September 2008

Abstract The particle-strengthened Cu–8 at.%Cr–4 at.% Nb alloy is processed by consolidation of atomized powders followed by extrusion to obtain bars and rolling to produce sheets. Comparison of copper matrix grain and second-phase particle structures in both extruded and rolled Cu–8Cr–4Nb was performed. Extruded material displayed locally banded arrangements of Cr_2Nb particles, while the distribution of particles was more uniform in rolled material. Mean Cr_2Nb particle sizes were found to be essentially the same for both processing methods. Non-spherical particles in the extruded alloy showed some preferred orientation, whereas the rolled material displayed a more uniform particle orientation distribution. Extruded material exhibited a dual grain size distribution with smaller grains in banded regions. The mean grain size of 1.36 μm in extruded material was larger than the 0.65 μm grain size of rolled material. A [101] texture was evident in extruded material, whereas the rolled material was only slightly textured along the [001] and [111] directions. The processing differences for the rolled and extruded forms give rise to different microstructures and hence higher creep strength for the extruded material in the temperature range of 773–923 K.

L. G. Vettraino · J. L. Heelan · C. A. Faconti · J. L. Walley · J. R. Groza · J. C. Gibeling (✉)
Department of Chemical Engineering and Materials Science, University of California, One Shields Ave., Davis, CA 95616, USA
e-mail: jcgibeling@ucdavis.edu

A. Garg
Glenn Research Center, NASA, 21000 Brookpark Rd. 49-1, Cleveland, OH 44135, USA

Introduction

Particle strengthening is an effective means of increasing the high temperature strength of metals. For applications such as the combustion chamber liner of the space shuttle main engine, rocket nozzle liners, and first wall diverter interactive components in fusion reactors requiring a combination of high strength and high thermal conductivity, materials based on a pure copper matrix with a dispersion of thermally stable second-phase particles are likely candidates. One such material is the NASA-developed GRCop-84 in which copper is alloyed with 8 at.% Cr and 4 at.% Nb, resulting in the formation of ~14 vol.% of the Cr_2Nb intermetallic. Most of the Cr_2Nb intermetallic phase precipitates as particles during rapid solidification from the melt. The precipitates formed directly from the melt (or 'primary' precipitates) are on the order of 0.5–1 μm in size [1]. Smaller, secondary Cr_2Nb intermetallic particles (<100 nm) precipitate from the solid solution. The Cr_2Nb intermetallic compound is stable up to its congruent melting point at 2006 K and has very low solubility in the solid copper matrix [2]. Good thermal conductivity is maintained as both the Cr and the Nb have negligible solubility in copper up to 1100 K [3, 4].

At moderate creep temperatures (773–923 K) it has been shown that the steady-state creep rate for extruded Cu–Cr_2Nb material is approximately an order of magnitude lower than that for rolled material [5]. To understand this difference in behavior a detailed microcharacterization study has been undertaken to compare relevant microstructural parameters (matrix grain size and particle size; shape and distribution; particle aspect ratio and orientation; and matrix grain texture) in the extruded and the rolled materials.

Experimental procedure

Materials

The extruded material used in this investigation was received as 25.4 mm diameter bars. The bars were manufactured by filling steel cans with −140 mesh (<106 μm) Cu–8Cr–4Nb alloy powders produced from conventional argon gas atomization [6]. The cans were then sealed and extruded at 1133 K using a round die with an approximate 30:1 reduction in area. The rolled material was fabricated by warm rolling sections of a 75 mm × 230 mm rectangular extruded bar, processed in a manner similar to the extruded material, from the initial thickness of 75 mm to 1 mm thick sheet. Each rolling pass consisted of a 15% reduction, with the initial pass starting at 673 K and subsequent passes continuing until the temperature had dropped to 473 K. The sheet was then reheated prior to the next series of rolling passes. The sheet was given a final 15-min anneal at 773 K followed by air cooling.

Specimen preparation

Specimens for microstructural analysis were sectioned from untested creep specimens that were cut parallel to the rolling or extrusion direction by wire EDM. The specimens from the extruded and rolled materials were mounted and prepared by standard metallographic techniques for scanning electron microscopy (SEM). Grinding from 320 to 2500 grit SiC paper was followed by a final polish using a 0.06-μm basic colloidal silica slurry on microfiber cloth. Specimens to be used for Cu matrix grain-size measurements were then etched.

The etchant for the extruded material consisted of 1.25 g of ammonium persulfate which was added to 175 mL of deionized water and 25 mL of concentrated ammonia. The extruded specimens were immersed into the etchant for 6 s. A different dilution and procedure were required for the rolled material. This etchant consisted of 2.5 g of ammonium persulfate which was added to 195 mL water and 5 mL of concentrated ammonia. Samples of rolled material were immersed in the etchant for 3 s. Finally, the specimens were rinsed in methanol followed by a deionized water rinse.

Specimens for Cr_2Nb particle size analysis were not etched since doing so preferentially attacks the copper matrix, leading to misrepresentation of the volume fraction and size of particles using standard quantitative image analysis techniques. The specimens for particle size analysis were ground and polished (as described above) then washed with 5% ammonia solution, rinsed in deionized water, rinsed with methanol and dried.

SEM was used for general microstructure imaging, Cu matrix grain size and particle counting, and size measurements for particles greater than 100 nm. Due to limited contrast between grains, the individual grains were outlined in Photoshop and then analyzed. Both grains and particles were measured for area assuming an elliptical shape using ImageJ software. The measured area of the ellipse was then equated to the area of a circle, and the final estimated diameter was calculated as the diameter of that equivalent circle. The image orientation was longitudinal for the sheet and the extrusion directions.

The same samples used for the SEM work were also analyzed by electron backscattered diffraction (EBSD) to determine mean Cu matrix grain size, shape, and orientation. Specimens for EBSD were prepared by grinding on 400–2400 grit SiC paper, polishing on diamond polishing film from 6 μm to 0.5 μm, and final polishing with 0.06-μm colloidal silica. Specimens were rinsed thoroughly (120 s) under cold running water between each step to remove any abrasive or polishing debris. The cold water rinse was followed with a deionized water rinse to remove impurities. The water was removed with a methanol rinse and the specimens were dried with a jet of warm air. As oil-based lubricants, Al_2O_3 polishing powder, and sonication all produce pitting they were avoided.

The smallest step size of 60 nm was used to detect the presence of grain boundaries via EBSD. A minimum two degree difference was necessary to distinguish between adjacent grains. An FEI XL30-SFEG SEM operating at 20 kV fitted with Field Emission Imaging (FEI) software and hardware including a Silicon Intensified Target (SIT) detector was used to capture standard SEM images in addition to texture information. Grain size distribution graphs were developed using TexSEM[1] Orientation Imaging Microscopy (OIM) imaging and analysis software. Grain sizes were measured over an observed area of 15 × 30 μm^2 and sorted into 60 bins distributed logarithmically over the range 0.01–5.7 μm.

For transmission electron microscopy (TEM), small discs approximately 10 mm in diameter were sectioned perpendicular to either the rolling or the extrusion directions. These samples were mechanically thinned to 200 μm and then punched into 3 mm disks. Those samples were further mechanically thinned to a final thickness of 100 ± 25 μm using a South Bay lapping fixture. Final thinning was conducted using a Struer's Tenupol-3 Jet Polisher. The electrolyte was 20 vol.% nitric acid in methanol, and its temperature was maintained at less than 250 K. An applied voltage of 10–15 V was used for polishing. A Philips CM120 TEM was used for general microstructure imaging, particle counting, and size measurements for particles less than 100 nm. Images of

[1] TexSEM software copyright EDAX division of AMETEK, Mahwah, NJ.

dislocations and dislocation/particle interactions were also captured utilizing TEM.

Results of microstructural characterization

General microstructure

SEM examination of the rolled material reveals a structure with a relatively uniform dispersion of both small and large particles (Fig. 1a). Small particles range from tens to hundreds of nanometers. Large particles are on the order of 1 μm and larger. Particles less than 100 nm cannot be observed by SEM. At this magnification, the sizes of the particles cannot be accurately measured, but the spatial distribution of the particulates can be observed.

In contrast, the extruded material shows a non-uniform distribution of particles (Fig. 2a). Regions sparsely occupied by particles alternate with those densely populated with particles. The two types of regions appear to occur in bands parallel to the extrusion direction. The thickness of the bands is typically 10–30 μm. It is hypothesized that the bands are prior individual powder particles that were elongated during extrusion.

TEM images of both the rolled and extruded Cu–8Cr–4Nb are shown in Figs. 1b and 2b, respectively. Both large (around 1 μm) and small (on the order of tens to hundreds of nanometers) particles are commonly observed in the Cu–8Cr–4Nb alloy. Such a bimodal distribution is observed regardless of the final alloy condition. Typically, the large particles are found at grain boundaries, whereas the small precipitates are found at grain boundaries and within the grains or subgrains. Twinning is observed in the Cr_2Nb particles in both the extruded and the rolled samples as shown in Fig. 3. These twins are likely associated with the transformation from the high-temperature hexagonal C15 form to the lower-temperature FCC C14 form of Cr_2Nb [4].

In addition, chromium particles are occasionally found, as shown in Fig. 4. These particles have been chemically identified in prior work by convergent beam analysis and have a different appearance (e.g., not twinned and

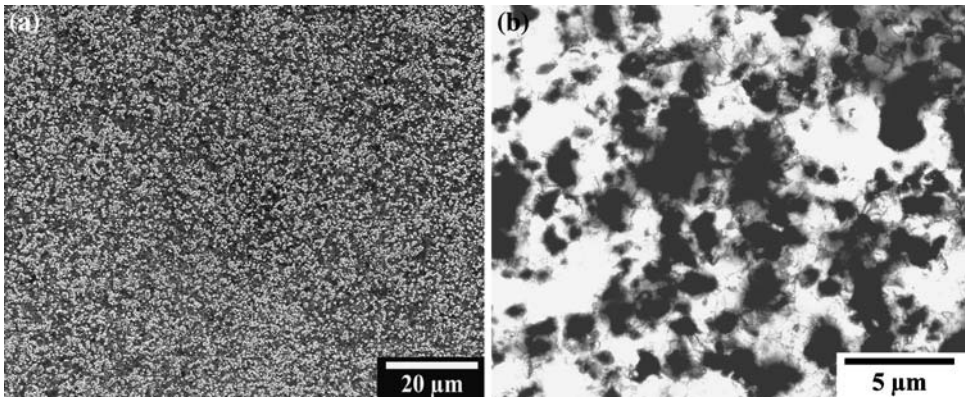

Fig. 1 SEM (**a**) and TEM (**b**) micrographs of the rolled Cu–8Cr–4Nb showing the distribution of the Cr_2Nb particles. The rolling direction and the longitudinal orientation are horizontal with respect to the SEM micrograph

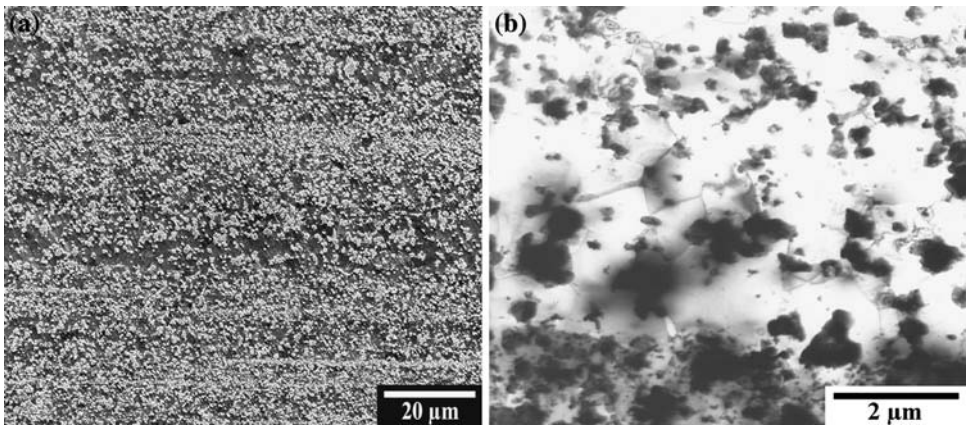

Fig. 2 SEM (**a**) and TEM (**b**) microstructures of the extruded Cu–8Cr–4Nb showing the distribution of the Cr_2Nb particles. The extrusion direction is horizontal with respect to the SEM micrograph. In the TEM microstructure, the predominantly small particles observed on top of the micrograph correspond to the "banded" regions with fewer large particles shown in the SEM. The extrusion direction in TEM is horizontal. Some subgrain boundaries are noticeable in the center of the TEM micrograph

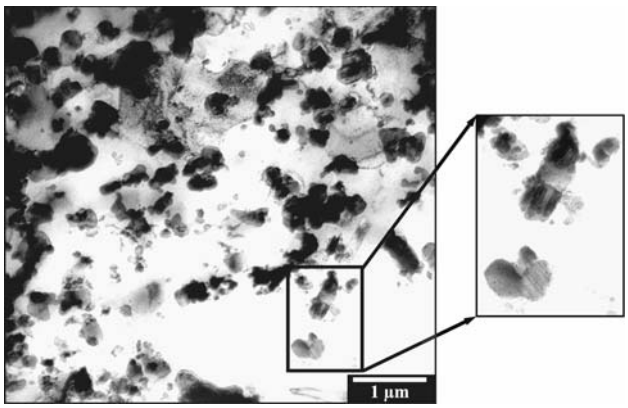

Fig. 3 TEM micrographs of rolled Cu–8Cr–4Nb showing twinning in Cr_2Nb particles. Twinned particles are shown in the inset

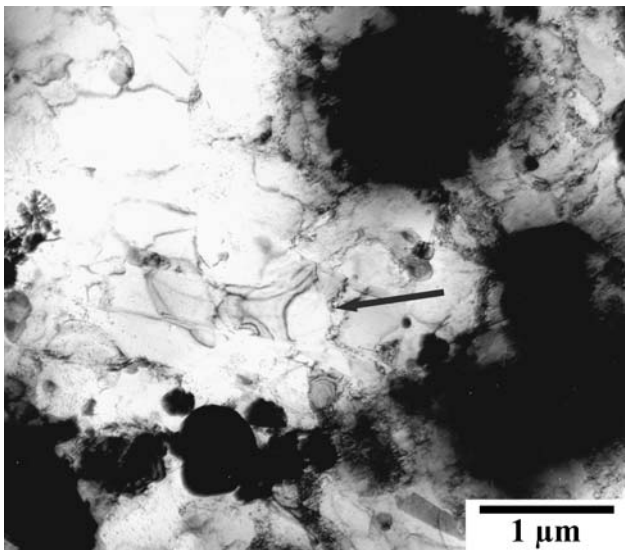

Fig. 4 TEM micrograph of rolled Cu–8Cr–4Nb alloy showing a Cr particle (*arrow*)

generally lower contrast) than the Cr_2Nb intermetallic [1, 7]. Observation of the Cr particles is an indication of a slightly higher Cr content than that required to form the stoichiometric Cr_2Nb compound. The Cr particles are consistent with the small excess of Cr in the alloy to minimize the Nb activity and the potential for hydrogen embrittlement [8].

Subgrain formation is evident in the extruded material (Figs. 2b, 5) but is less developed in the rolled material. Figure 6 is a TEM micrograph showing the dislocation structure in the rolled sample with the incipient substructure formation. Individual dislocations, dislocation arrays, and networks are also apparent at these magnifications, with the rolled condition displaying an overall higher dislocation density than the extruded form.

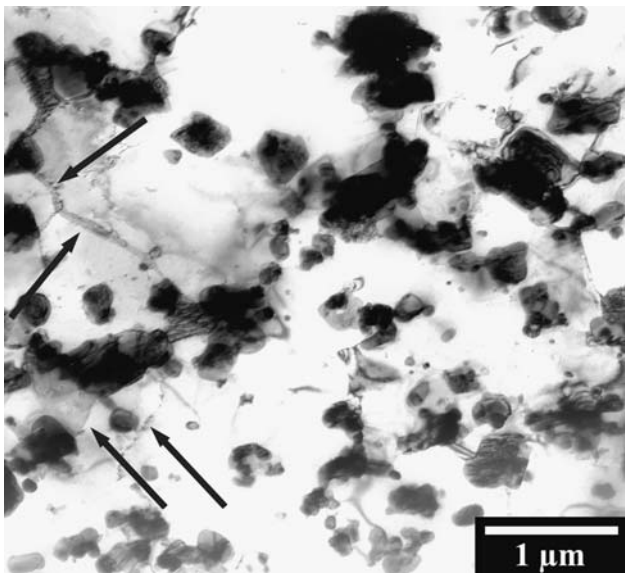

Fig. 5 TEM micrograph of Cu–8Cr–4Nb that shows a higher tendency to form subgrains in the extruded sample than in the rolled sample (Fig. 6). Arrows show well-developed subgrain boundaries

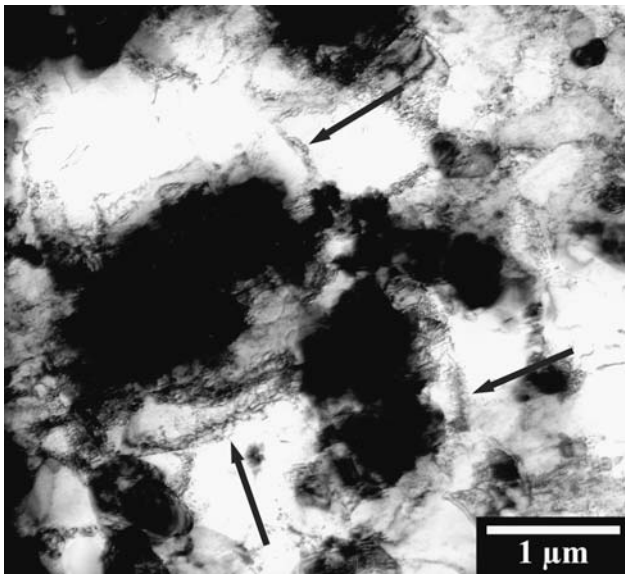

Fig. 6 TEM micrograph of Cu–8Cr–4Nb alloy showing the dislocation structure and incipient subgrain formation in the rolled sample. Arrows show loosely formed subgrain boundaries

Particle size and distribution

The size distribution of the Cr_2Nb particles for the rolled material is shown in Fig. 7a. The total area fraction is 14.1% for all particles, which is in very good agreement with the volume fraction calculated using the average chemistry for commercially produced GRCop-84. From the TEM images,

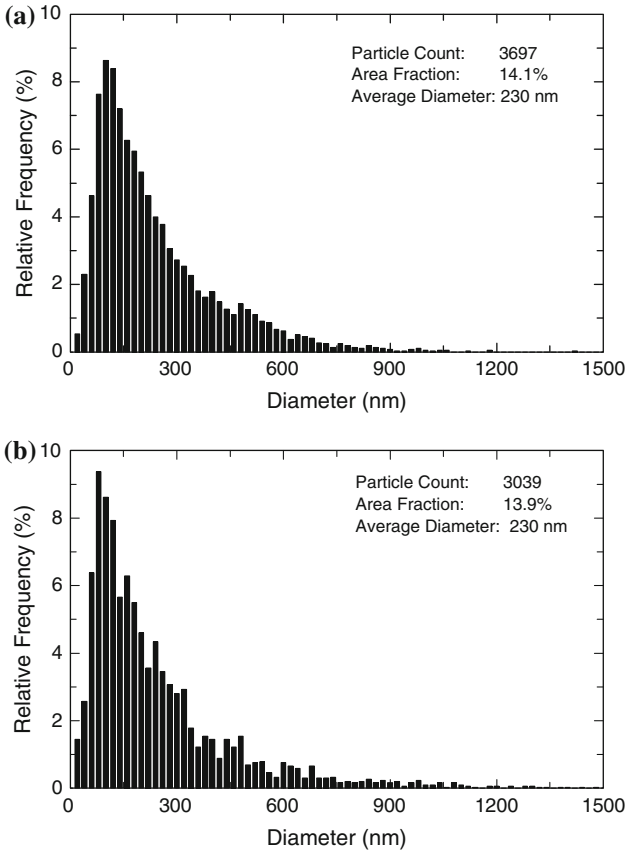

Fig. 7 Graph of the relative frequency versus particle diameter for the rolled (**a**) and extruded (**b**) conditions

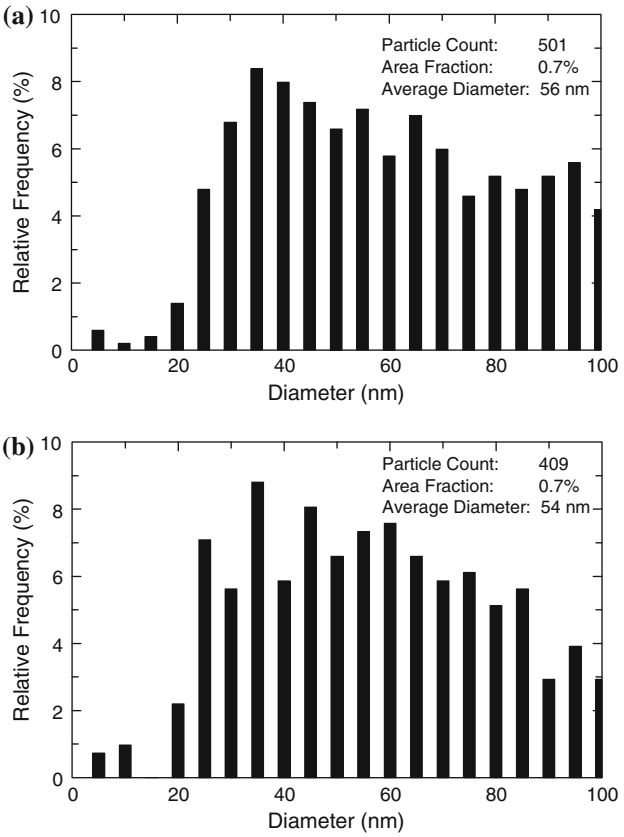

Fig. 8 Graphs of the relative frequency versus particle diameter for sizes of 100 nm and less for the rolled (**a**) and extruded (**b**) materials

the area fraction of particles of sizes 100 nm and smaller, that is, those within grain interiors, was measured to be 0.7%. These "small" particles play a critical role in resisting dislocation motion in grain interiors to provide creep resistance; their size distribution is shown in Fig. 8a. Particles larger than 100 nm, measured from SEM micrographs, are designated as "large" particles. As shown in Fig. 7a, the majority of the particles have sizes smaller than 300 nm with a continuous decrease in the number of particles as size increases.

The particle size distribution for the extruded Cu–8Cr–4Nb (Fig. 7b) is very similar to the rolled material. Both the extruded and the rolled distributions maintain a log-normal distribution. However, the frequency of particles smaller than 300 nm in diameter is slightly less in the extruded (Fig. 7b) than in the rolled (Fig. 7a) material. The total particle area fraction of 13.9% corresponds fairly well with that of the rolled material, and 0.7% of the particles are again equal to or smaller than 100 nm in diameter (Fig. 8b). The average particle size of the extruded Cu–8Cr–4Nb (230 nm) is the same as that of the rolled material (230 nm). These and other measured and calculated matrix grain- and Cr_2Nb particle-related parameters are summarized in Table 1, including statistical error data.

Particle aspect ratio and orientation

Although the particle shape is close to equiaxed, a slight elongation of the large primary particles is noticeable. For particles larger than 100 nm the aspect ratio is given as the particle length, *b*, divided by the particle width, *a*. A plot of the relative frequency versus aspect ratio for the rolled material is shown as Fig. 9a. The aspect ratios range from 1.0 for round particles to approximately 4 with the largest frequency situated between 1.0 and 2.0 with an average ratio of $\sim$1.53. The relative frequency versus the aspect ratio for the extruded Cu–8Cr–4Nb is shown in Fig. 9b. Similar to the rolled material the greatest concentration of the aspect ratios lies between 1.0 and 2.0. A greater relative frequency for those data close to 2.0 or above is shown. This accounts for an average aspect ratio of 1.70 for the extruded material, indicating the particles for the extruded form appear slightly more elongated than those in the rolled material.

Since the particles are non-spherical, their orientation angle can be measured from the particle major axis with respect to either the rolling or the extrusion direction. The relative frequency of the particle orientation for the rolled Cu–8Cr–4Nb plotted against angle is presented in Fig. 10a.

Table 1 Summary of measured microstructural parameters for Cu–8Cr–4Nb

Microstructure parameter	Rolled		Extruded	
	Average	95% confidence interval	Average	95% confidence interval
Matrix grain size (μm)	0.65	±0.053	1.36	±0.071
Matrix grain texture	[001], [111]	–	[101]	–
Particle size (nm)				
Large particles (>100)	230	±12.5	230	±11.0
Small particles (<100)	56	±3.0	54	±2.6
Volume fraction (%)				
Large particles	13.4	±1.61	13.2	±1.02
Small particles	0.7	±0.08	0.7	±0.05
Particle aspect ratio				
Large particles	1.53	±0.023	1.70	±0.029
Interparticle spacing (μm)				
Large particles	0.49	±0.081	0.48	±0.066
Small particles	0.53	±0.077	0.50	±0.056

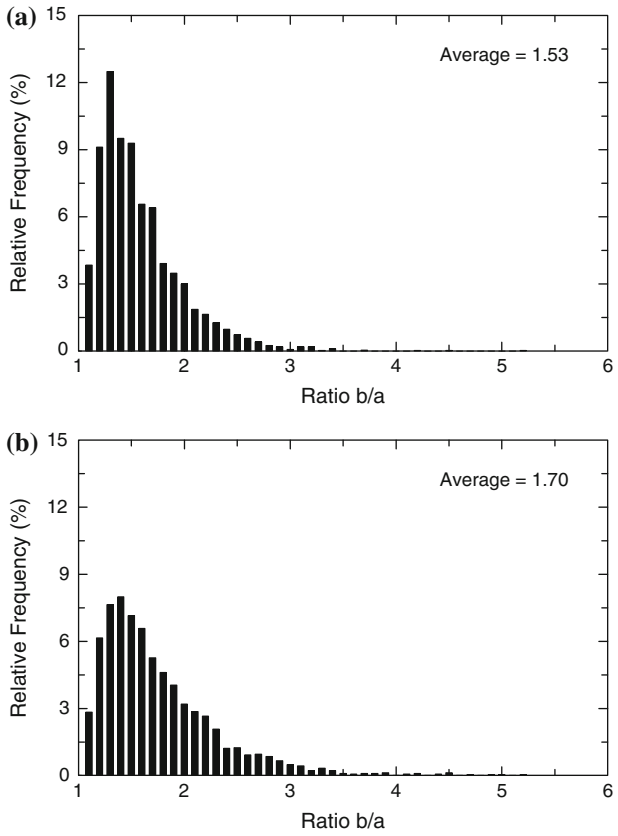

Fig. 9 Graphs of the relative frequency versus aspect ratio *b/a* for particles in the rolled (**a**) and extruded (**b**) conditions

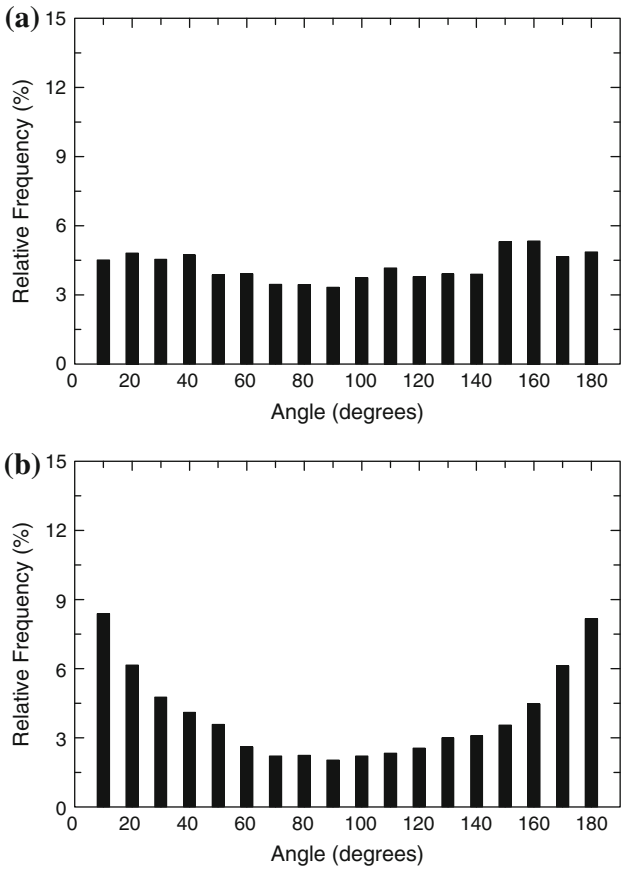

Fig. 10 Plots of relative frequency versus angle of major axes of particles relative to extrusion/rolling direction for the rolled (**a**) and extruded (**b**) materials

Very little deviation in frequency is shown for any angle ranging from 0° to 180°. This is in contrast to the orientation of particles in the extruded material that is illustrated in Fig. 10b. The relative frequency for the extruded condition is shown to be higher in the 0°–30° and 150°–180° ranges, which correspond to the extrusion direction. In the middle ranges, the relative frequency is less than 3%, but at the high and low ends it exceeds 8%.

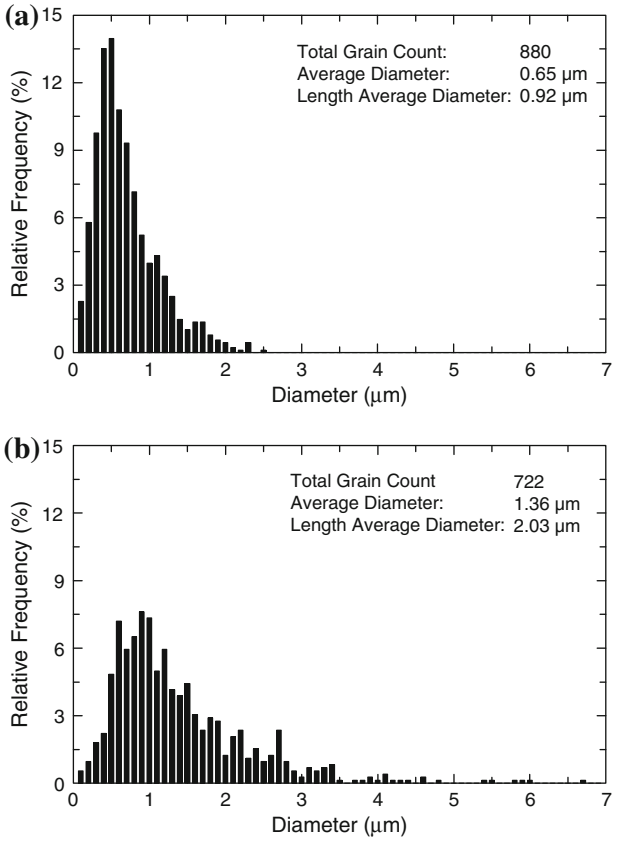

Fig. 11 Graphs of relative frequency versus grain diameter for the rolled (**a**) and extruded (**b**) conditions

Copper matrix grain size, shape, and orientation

Relative frequency versus Cu matrix grain diameter is plotted in Fig. 11 for both the rolled and the extruded materials. Figure 11a is a plot of the distribution of grain sizes for the rolled Cu–8Cr–4Nb alloy. The mean grain diameter based on equivalent areas is 0.65 μm. Figure 11b illustrates the relative number of grains versus grain diameter for the extruded material. In this case, the mean grain diameter was found to be 1.36 μm. The graphs of the relative frequency versus grain size for the extruded and rolled materials display log-normal distributions. The grain-size distributions of Fig. 11 indicate that the grains for the rolled material are between 0.1 and approximately 2.6 μm, while the grain size range for the extruded materials is larger (from 0.1 to greater than 6.6 μm diameter). These ranges suggest that grain size is limited by the spacing of the large Cr_2Nb particles (Figs. 1, 2). For the extruded material, the average grain size in the banded regions is 1.15 μm, as compared to 1.65 μm in the regions with fewer particles.

The color grain map obtained by EBSD for the rolled material (Fig. 12a) shows that the grains are elongated with respect to the rolling direction whereas grains for the extruded Cu–8Cr–4Nb show the grain shape to be largely equiaxed, as displayed in Fig. 12b. While it is difficult to distinguish the two phases in EBSD because of the similarity of their crystal structures, the phase maps for the two material conditions reveal the more uniform distribution of Cr_2Nb particles in the rolled material as compared to the banding of the extruded material noted in the SEM images. The inverse pole figure maps with respect to the [001] pole are also shown in Fig. 12. The respective red- and blue-colored grains in Fig. 12a show a very slight texturing in the [001] and the [111] directions for the rolled material. The predominant green color for most of the individual grains indicates strong texturing in the [101] direction for the extruded material (Fig. 12b).

Discussion

In some aspects, final processing by either rolling or extrusion results in similar microstructures, e.g., large and small Cr_2Nb particles in a copper matrix with micron-sized grains. On average, though, the grain size for the extruded GRCop-84 material was twice that of the rolled form. In other aspects, differences are noticed between these microstructures, which are likely related to the differences in processing methods. As shown in Fig. 2, a banded distribution of particles is observed in the extruded material while the rolled material (Fig. 1) displays a very homogenous distribution of particles. It appears that the total reduction in thickness (up to 99%) during rolling redistributed the precipitates as the copper matrix flowed around the hard Cr_2Nb particles.

The banding from the extrusion process consists of an uneven size and spatial distribution of particles. These bands may be related to the initial alloy powder particles. During extrusion of the powders into rods, the powder particles would be elongated by approximately 30:1 while the diameter would be decreased by about 5:1. For the average powder particle diameter of 35 μm, this would result in a band on the order of 1 mm long and 7 μm thick. Variations in cooling rates between powder particles and individual powder particle chemistry can affect the size and volume fraction of Cr_2Nb. These variations may result in the small scale variability of Cr_2Nb particle spatial distribution observed in the extruded material.

On the other hand, since the rolled Cu–8Cr–4Nb is processed from the extruded bar, it is apparent that the further processing caused by rolling creates a more uniform Cr_2Nb particle spatial distribution. During rolling, the softer copper matrix flows around the harder Cr_2Nb intermetallic particles. More deformation will occur initially in the areas with fewer particles (and larger Cu grains) since those local regions are less affected by both the Hall-Petch

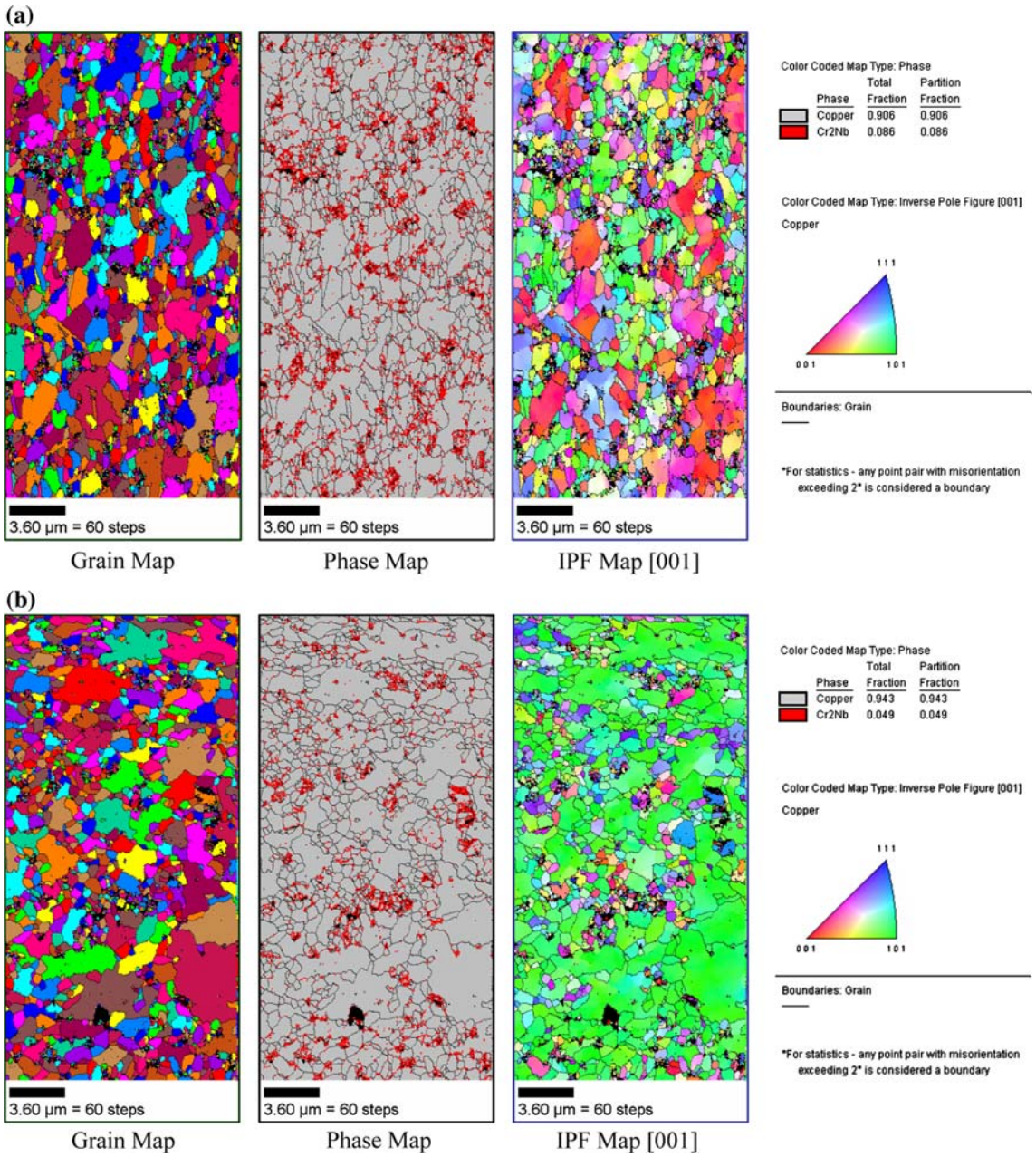

Fig. 12 Grain map, phase map, and inverse pole figure for Cu–8Cr–4Nb in the rolled (**a**) and extruded (**b**) conditions. The rolling direction is vertical, while the extrusion direction is horizontal with respect to each of the maps

and Orowan strengthening mechanisms [9]. As the bands are flattened, the spatial distribution of the particles will become more uniform. Additional microstructural refinement can also occur due to agglomerations of Cr_2Nb particles (formed in the liquid by weakly fusing together) being broken apart by shearing forces generated during rolling. The break up of agglomerations of Cr_2Nb particles will also contribute to the decrease in the relative frequency of the largest particle sizes as seen in Fig. 7.

In the extruded material, the grain size is directly related to the particle distribution, i.e., it is smaller in the regions where the large particle number density is higher. Conversely, the regions with fewer large particles have larger grain sizes. One possible explanation is that grain growth following recrystallization occurs in regions of low particle density but is impeded in regions with high densities of particles. That is, the effect of particles is to act as pinning centers for grain boundary migration after recrystallization of the deformed matrix. Deformation of the matrix from the extrusion or rolling process would act as the driving force for nucleation and subsequent grain refinement (recrystallization).

The observed Cr_2Nb particle sizes are consistent with second-phase particle size data reported in previous studies of Cu–8Cr–4Nb [1, 10]. The particle size distribution for the rolled Cu–8Cr–4Nb shows a trend similar to the extruded Cu–8Cr–4Nb. The particles are shown to continually increase in frequency as they approach 100 nm diameter (Fig. 7). These data suggest that, in general, the particulate sizes do not change significantly with the specific forming process. It is noted that the mean particle diameter (230 nm) is the same for the rolled material as for the extruded (230 nm). This similarity in mean diameter indicates the rolling process has little effect on the overall average particle size. The Cr_2Nb interparticle spacing, λ, is related to the length, b, the thickness, a, and the volume fraction, f, of the particulate as expressed by [11]:

$$\lambda = (ab/f)^{1/2} \quad (1)$$

The mean interparticle spacing for particles greater than 100 nm in length has been calculated as 0.49 μm for the rolled material, which is the same as that of the extruded material, 0.48 μm. Similarly, the mean interparticle spacing for particles less than 100 nm is calculated to be 0.53 μm for the rolled material, which is the same (within experimental error) as that for the extruded material (0.50 μm). The calculated interparticle spacing results differ from the measured Cu matrix grain sizes. That is, thermo-mechanical processing allows for grain growth in the extruded form to a larger size than that of the rolled material. The particles in the rolled form may more effectively pin the grain boundaries, due to the more uniform distribution. Both the rolled and the extruded materials have the same particle size and interparticle spacing, indicating the extra deformation steps for the rolled material have little effect on particle refinement. In general, the larger Cr_2Nb agglomerates may be more efficiently broken down to smaller particles (as shown in Fig. 7). Relative to the extrusion processing this is shown by the increased frequency of smaller particles (<100 nm).

However, the average particle aspect ratio for the rolled material (1.53) is smaller than that of the extruded form (1.70). Because the average particle size and spacing are the same in both the extruded and rolled materials, it is surmised that the apparent change in particle aspect ratio is actually a result of a change in particle orientation. In this situation the particle aspect ratios are influenced by extrusion, which tends to align the particle length, b, with the extrusion direction. As a result the aspect ratios, b/a, are increased. This conclusion is confirmed by the observation that the rolled material exhibits a uniform orientation of larger particles with respect to the rolling direction. This is in contrast to a preferred orientation of the elongated particles in the extruded specimens. Since the shape of the second phase particles only changed minimally, this should have little effect on the creep strength of the alloy.

Consistent with an extra recrystallization step, the average grain size for the rolled material (0.65 μm, Fig. 11a) is smaller than that for the extruded material (1.36 μm, Fig. 11b). The maximum grain size of almost 7 μm for the extruded Cu–8Cr–4Nb is much larger than the maximum grain size of approximately 2.6 μm for the rolled material. The grain size difference can be explained in terms of recrystallization and grain growth behavior. The Cu–8Cr–4Nb extruded material can quickly recrystallize by deformation at 1133 K. It is suggested that the multiple passes during subsequent rolling may allow for some recrystallization but limited grain growth. The recrystallization temperature for pure copper may be taken as approximately 500 K, but will depend largely on the amount of prior cold working and defect concentration [12]. This is near the upper limit of the warm rolling (573 K) and well below the annealing temperature of 773 K. The rolled material goes through a series of rolling passes followed by a 15-min anneal at 773 K. As shown by Fig. 13, only recovery and partial recrystallization of rolled Cu–8Cr–4Nb has occurred after annealing at 773 K for 30 min in 23% cold-rolled sheet [13]. Microstructural evidence by Ellis and Garg shows that full subgrain structure develops in only 30 min at 873 K [13]. Therefore, the rolled material is only partially recrystallized, as shown by the elongated grains in Fig. 12a and the presence of many dislocations (Figs. 4, 6). This suggests that grain growth in the rolled material in this study does not occur or is limited to temperatures above 873 K during a 30-min anneal.

Smaller grain sizes will provide a more effective barrier to dislocation motion and hence should increase the yield strength of the rolled alloy relative to the extruded alloy. However, grain size should only have an influence on creep results in the range of temperatures and stresses at which diffusion is the rate controlling mechanism; for creep

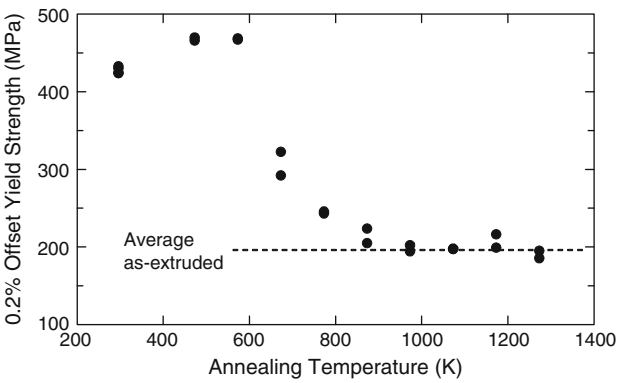

Fig. 13 Effect of annealing temperature on room temperature yield strength of 23% cold-rolled Cu–8Cr–4Nb alloy [13] for 30 min anneals

controlled by dislocation glide and interaction with particles, the small differences in grain size reported here should have a minimal impact. Further, the preferential orientation of the matrix grains should help to increase the creep strength of the GRCop-84 alloy. Such an orientation will provide more barriers to dislocation motion since generalized strain cannot be accommodated.

Very slight texturing with respect to the [001] and the [111] directions was found for the rolled material and strong texturing in the [101] direction was observed in the extruded material. To account for this difference, the warm rolling and annealing must have removed the texturing induced by the extrusion process. Rolling was performed bi-axially, which effectively leads to recrystallization that eliminates the strong texture in the extruded material.

Summary and conclusions

Based on the results of the microstructural study presented above, the following observations can be made:

1. A uniform microstructure was evident at relatively low magnifications in the rolled Cu–8Cr–4Nb material, but second-phase particle and Cu matrix grain size banding was found in the extruded material. The banding is identified with regions that contained high particulate density, coupled with smaller matrix grain sizes.
2. Most of the Cr_2Nb particles range from 100 to 300 nm in size, with average diameters measured to be $\sim$230 nm for both the rolled and the extruded Cu–8Cr–4Nb materials.
3. The particulates in both the rolled and the extruded materials were shown to be slightly elongated, having small aspect ratios averaging 1.53 for the rolled product and 1.70 for the extruded form. The largest aspect ratio is found in the extruded material (up to approximately 5). However, the apparent difference in the average aspect ratios is attributed to differences in particle orientation. The extrusion process slightly increases the primary particle's elongation in the extrusion direction.
4. The rolled material exhibited little to no preferred orientation (of the major axes) of particles relative to the rolling direction. The particles in the extruded alloy showed a preferred orientation along the extrusion direction.
5. The grains in the rolled Cu–8Cr–4Nb were somewhat elongated in the rolling direction whereas those of the extruded material were mostly equiaxed.
6. The average grain size for the rolled material was 0.65 μm, while the average grain size for the extruded material was 1.36 μm, which was twice that for the rolled material.
7. By using EBSD, minor texturing along the [001] and [111] directions was found for the rolled material while strong texturing in the [101] direction was evident for the extruded material.
8. Since the average grain size for the extruded form is only twice that of the rolled form, the major influence to creep strength must be texturing.

Acknowledgements This work was funded as part of NASA Grant NCC3-859. The authors wish to thank Drs. David Ellis and Michael Nathal for their continuing support and advice regarding this project. The authors also wish to express their appreciation to Dr. George Kaschner of the Los Alamos National Laboratory for the kind use of the SEM/EBSD equipment, which resulted in the OIM images used in this study.

References

1. Anderson KR, Groza JR, Dreshfield RL, Ellis D (1993) Mater Sci Eng A 169:167–175
2. Venkatraman M, Neumann JP (1986) Bull Alloy Phase Diagrams 5:462–466. doi:10.1007/BF02867811
3. (a) Chakrabati DJ, Laughlin DE (1982) Bull Alloy Phase Diagrams 2:507; (b) Chakrabati DJ, Laughlin DE (1984) Bull Alloy Phase Diagrams 5:59, 99
4. Thoma DJ, Perepezko JH (1992) Mater Sci Eng A 156:97–108
5. Decker MW, Groza JR, Gibeling JC (2004) Mater Sci Eng A 369:101–111
6. Ellis DL, Michal GM (1999, Sep) NASA Contractor Report 185144
7. Ellis DL, Misra AK, Dreshfield RL (1996) In: Thompson AW, Moody NR (eds) Proceedings of the fifth international conference on the effect of hydrogen on the behavior of materials. TMS, Warrendale, pp 1049–1056
8. Anderson KR, Groza JR, Dreshfield RL, Ellis D (1995) Metall Mater Trans A 26:2197–2206. doi:10.1007/BF02671235
9. Anderson KR, Groza JR (2001) Metall Mater Trans A 32:1211–1224. doi:10.1007/s11661-001-0130-x
10. Decker MW (2003) Constant stress creep properties of extruded Cu-8Cr-4Nb (GRCop-84). M.S. Thesis, University of California, Davis
11. Kelly PM (1973) Int Met Rev 18:31
12. Shewmon PG (1983) Transformations in metals. J. Williams Book Company, Oklahoma, pp 69–125
13. Ellis DL, Garg A (to be published) Annealing behavior of GRCop-84. NASA Technical Memorandum. NASA Glenn Research Center, Cleveland, OH